

High-throughput size-based rare cell enrichment using microscale vortices

Soojung Claire Hur, Albert J. Mach, and Dino Di Carlo^{a)}
 University of California, Los Angeles, California 90095, USA

(Received 2 December 2010; accepted 26 January 2011; published online 29 June 2011)

Cell isolation in designated regions or from heterogeneous samples is often required for many microfluidic cell-based assays. However, current techniques have either limited throughput or are incapable of viable off-chip collection. We present an innovative approach, allowing high-throughput and label-free cell isolation and enrichment from heterogeneous solution using cell size as a biomarker. The approach utilizes the irreversible migration of particles into microscale vortices, developed in parallel expansion-contraction trapping reservoirs, as the cell isolation mechanism. We empirically determined the critical particle/cell diameter D_{crit} and the operational flow rate above which trapping of cells/particles in microvortices is initiated. Using this approach we successfully separated larger cancer cells spiked in blood from the smaller blood cells with processing rates as high as 7.5×10^6 cells/s. Viable long-term culture was established using cells collected off-chip, suggesting that the proposed technique would be useful for clinical and research applications in which *in vitro* culture is often desired. The presented technology improves on current technology by enriching cells based on size without clogging mechanical filters, employing only a simple single-layered microfluidic device and processing cell solutions at the ml/min scale. © 2011 American Institute of Physics. [doi:10.1063/1.3576780]

I. INTRODUCTION

Selective target cell isolation based on intrinsic biomarkers, such as size, deformability, and polarizability, allows for cost-effective detection and purification of viable cells with unknown molecular biomarkers and without immunolabeling. Moreover, high purity collection of intact rare cells with preserved gene expression will facilitate molecular assays for such cells, potentially useful for cell biology research, immunology, tissue engineering, and medicine. In the field of the tissue engineering, for instance, there is intense interest in purification of specific cell populations for high quality tissue graft construction, but the limited knowledge of the specific surface markers required for discrimination of such cells remains a challenge.¹ More generally, immunostaining² and transgenic³ enrichment techniques are not desired for some research and clinical applications, which require to collect viable cells with preserved gene expression profiles. Additionally, techniques capable of isolating rare cells in peripheral blood, such as fetal cells,⁴ endothelial progenitor cells,⁵ and circulating tumor cells (CTC),⁶ in a label-free manner with high-throughput, will have an immediate impact for diagnostic and prognostic applications. Therefore, systems that allow cost-effective, label-free, and high-throughput target cell enrichment will have significant impact on both clinical and research applications.

Recently, there have been several efforts to develop microfluidic platforms for label-free separation of target cells utilizing intrinsic physical and electrical biomarkers.⁷ The most widely adopted physical biomarker is cell size. Many microfluidic techniques for continuous size-based enrichment, including membrane microfiltration,⁸ pinched flow fractionation,⁹ deterministic lateral

^{a)}Electronic mail: dicarlo@seas.ucla.edu.

displacement,^{10–12} and hydrophoresis,¹³ have been demonstrated for numerous potential applications. Applications include the fractionation of whole blood,^{11,12} cardiomyocyte enrichment for cardiac graft construction,¹⁰ size-based cell cycle synchrony,¹³ as well as CTC separation from blood.⁸ These approaches have been shown to be successful in prototype systems, however, in many cases the throughput required for commercial applications would require parallelization, or in the case of filtration approaches, samples are not easily moved or handled after separation. Recent work in inertial focusing offers rapid size-based separation at the ml/min scale but lacks the ability to significantly concentrate the target population into a smaller volume after operation.^{14–16}

Trapping of particles by size in laminar vortices may address these previous shortcomings. The presence of laminar vortices resulting from inertially driven separation of the laminar boundary layer at sharp corners has been observed in previous computational and theoretical studies.^{17,18} Mesoscale laminar vortices have been extensively studied to understand the aggregation of red blood cells (RBCs) and platelets within a vortex^{19–21} and particle motion in a recirculation zone has been presented in alveolar flow.²² Interaction of particles and vortices at the microscale has been further investigated by observing pattern formation of recirculating colloidal particles by Lim *et al.*²³ Similar pattern formation and effects of vortices on motility were reported for swimming micro-organisms sequestered in vortices formed in microfluidic devices.²⁴ Microscale laminar vortices were also utilized to broaden cell/particle free layers useful for high-purity plasma extraction²⁵ or to enhance the lateral displacement of ordered particle streams based on size.²⁶ However, for particulate samples in microfluidic systems, it has been considered difficult to achieve initial trapping of relatively large bioparticles in the vortices without the aid of external forces.^{27,28} Recently, work by Khabiry *et al.*²⁹ has investigated target cell migration and immobilization into microscale vortices, but in this case entry into the vortices was due to gravitational force. Accordingly, this method separates on a combination of both cell density and size and requires a slow enough flow rate such that gravitational effects are significant.

Here, we present a passive, continuous microfluidic device that isolates larger target cells into the microscale vortices from a heterogeneous suspension with high-throughput (7.5×10^6 cells/s) by instead exploiting differences in shear-gradient induced lift forces using an array of expansion-contraction channels. First, we systematically varied the flow rate to determine when the microscale vortex formation is initiated and stabilized. Then, the critical diameter required for trapping particle/cells in vortices was identified using particle/cells with various diameters. Furthermore, as a proof-of-concept toward the enrichment of larger cancer cells from smaller blood cells, cultured cancer cells, spiked in a dilute blood sample prior to the injection, were separated and enriched using our approach. Viability of the collected cells was monitored in order to determine whether the proposed fluidic process adversely affects processed cells. Utilizing unique microscale fluid dynamics, the presented technique provides a simple and practical size-based cell enrichment approach for a variety of applications.

II. PARTICLE TRAPPING MECHANISM

In this study, we utilized microscale laminar vortices combined with inertial focusing to selectively isolate and trap larger cells of interest (e.g., cancer cells) while smaller cells (e.g., erythrocytes and leukocytes) are flushed out of the device. Multiple microscale laminar vortices (i.e., Moffatt's corner eddy flow¹⁷) were created by flowing the particle-laden fluid sample at sufficiently high channel Reynolds number, $R_c = \rho U_m D_h / \mu$, through a channel consisting of an array of expansion-contraction reservoirs placed in series and parallel [Figs. 1(a) and 1(b)]. Here, ρ , U_m , and μ are the density, maximum velocity, and dynamic viscosity of the fluid, respectively, while D_h is the hydraulic diameter of the channel, defined as $D_h = 2W_c H / (W_c + H)$, where W_c and H are the width and height of a straight focusing channel, respectively. Upstream of the vortices, particles migrate to distinct vertical and lateral equilibrium positions resulting from a balance between two counteracting inertial lift forces, namely, a shear-gradient lift F_{LS} and a wall effect lift F_{LW} (Ref. 30) [see Fig. 1(d)]. Previous work suggests that the shear-gradient lift force scales as $F_{LS} = f_L \rho U_m^2 a^3 / W_c$, acting on particles and leading to migration toward the channel walls, whereas

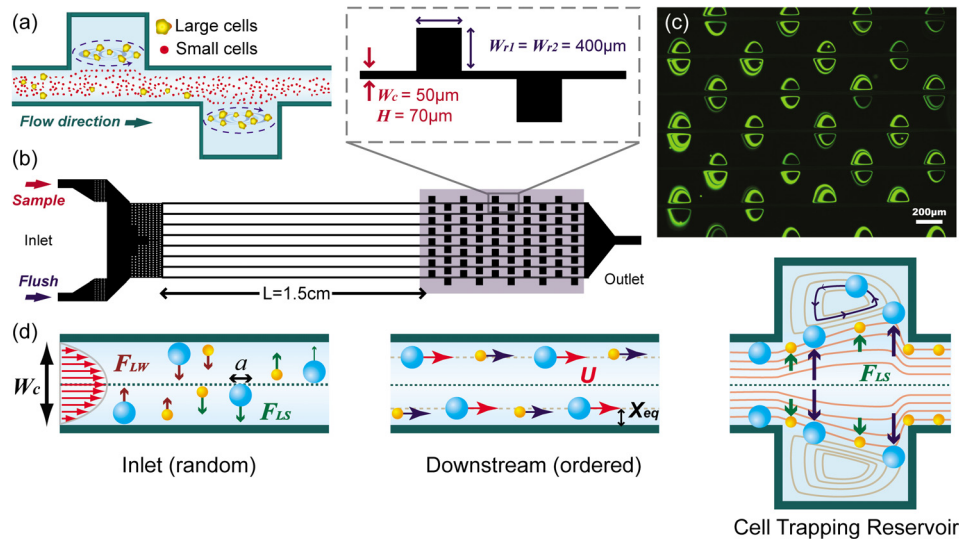


FIG. 1. Device design and working principle. (a) The schematic describes that larger cells are trapped in the reservoir while smaller cells freely pass through the reservoir region due to difference in the lift forces that cells encounter. (b) The device consists of eight parallel high aspect ratio straight channels ($50 \times 70 \mu\text{m}$) with ten cell trapping reservoirs ($400 \times 400 \times 70 \mu\text{m}$) in each channel. (c) Parallel trapping of $10 \mu\text{m}$ fluorescent particles in microscale vortices. (d) A particle with diameter a experiences wall effect lift F_{LW} and shear-gradient lift forces F_{LS} , in straight channels, resulting in a dynamic lateral equilibrium position X_{eq} and uniform particle velocities U . Here, X_{eq} is defined as the distance between the center of particles/cells and the channel walls. At the reservoir, larger particles experiencing larger F_{LS} are pushed toward the vortex center and trapped, whereas smaller particles are flushed out of the region.

the wall effect lift force, scaling as $F_{LW} = f_L \rho U_m^2 a^6 / W_c^4$, repels the particles away from the wall.³¹ Here, f_L , a , and W_c are the dimensionless lift coefficient, the particle diameter, and the channel width (i.e., shorter face of the rectangular channel), respectively. By using a straight channel with rectangular cross-section, the dynamic equilibrium positions of the flowing particles/cells can be precisely controlled to be in the proximity of the channel walls at uniform height for a finite R_c .³² As the entrained particles enter a reservoir, where the neighboring wall is no longer in close proximity, the particles are exposed only to a shear-gradient lift F_{LS} in the direction toward the vortex center.²⁶ Since the shear-gradient lift force scales with a^3 , larger particles experience a larger lateral lift force. This force is assumed to be balanced by Stokes drag, $F_d = 3\pi\mu a v_t$, thus the lateral migration velocity v_t will scale with a^2 and be independent of the particle mass. Size-dependent lateral migration drives particles across streamlines past the detached boundary (separatrix) toward the vortex core where they remain isolated and orbiting in the vortex. This leads to the possibility of size-selective trapping, as below a particle size cutoff, particles do not migrate at a sufficient rate to pass the separatrix and remain in focused streams, flowing out of the device. The high flow rate required for vortex generation assists in this process as theoretical analysis has showed that the lateral equilibrium position of focused particles shifts toward the wall as R_c increases,³³ bringing the focused streams of flowing particles/cells closer to the separatrix at the reservoir and possibly enhance the capturing efficiency.

III. MATERIAL AND METHODS

A. Device design and fabrication

To determine the device operational parameters, such as flow rate and critical diameter for trapping, we implemented a single straight high-aspect ratio channel ($W_c = 50 \mu\text{m}$, $H = 70 \mu\text{m}$, and $L = 4.5 \text{ cm}$), consisting of one inlet with coarse filters, two reservoirs ($W_{R1} = W_{R2} = 400 \mu\text{m}$), and one outlet. The high-aspect ratio straight channel was implemented so that flowing particle/cells were inertially focused to two distinct lateral focusing positions closer to channel walls at a

uniform z-plane³² prior to entering the cell trapping reservoir region. For label-free target cell isolation, we designed a microfluidic chip with two inlets, eight parallel straight channels with aforementioned dimensions, and one outlet. The simplicity of the device (a single rectangular channel with reservoirs) allowed the system to be easily parallelized in order to enhance the throughput [Fig. 1(c)]. Moreover, a simple two-inlet system allowed for easy and rapid solution exchange within the device, providing a means to flush untrapped, contaminating smaller blood cells and to enhance the final enrichment ratio and the purity of the collected samples. The reservoirs were placed in an alternating pattern in order to place the maximum number of reservoirs in a given compact footprint.

The microfluidic devices were fabricated with conventional soft lithography techniques using polydimethylsiloxane (PDMS).³⁴ In brief, for mold fabrication, a 4" silicon wafer was spin-coated with a 70 μm thick layer of a negative photoresist (KMPR 1050, Microchem), exposed to UV-light through a designed Cr-photomask and developed. PDMS (Sylgard 184, Dow Corning) was cast on to the prepared mold and degassed. Cured PDMS cast was separated from the mold and the inlet and outlet were punched with a pin vise (Pin vise set A, Technical Innovations Inc.). The punched PDMS chip was bonded to a slide glass by exposing both PDMS and a slide glass surfaces to air plasma (Plasma Cleaner, Harrick Plasma) to enclose the microfluidic chips.

B. Particle and cell suspension preparation

Internally dyed fluorescent polystyrene microspheres were purchased from Duke Scientific. Samples with particles, whose diameters are 9.9 μm (Product No. G1000, CV < 5%), 4.8 μm (Product No. G0500, CV < 5%), and 1 μm (Product No. R0100, CV < 5%), were prepared by diluting the particle suspensions to 0.1%v/v with deionized water containing 0.1%w/v Tween 80 (Fisher Chemical). HeLa cells (a cervical carcinoma cell line) and MCF7 cells (a breast carcinoma cell line) were cultured in the growth media suggested by American Type Culture Collection (ATCCTM) and incubated at 37 °C in 5% CO₂ until near confluence. The concentration and the size distribution of cell suspensions were measured using a Coulter Counter (Z2TM Coulter Counter[®], Beckman Coulter). Various concentrations of fluorescently stained live HeLa cells (Calcein AM) were loaded into the device with 80 reservoirs placed in parallel and series to evaluate the capturing efficiency and viability of captured and released cells. For spiking experiments, cancer cells (HeLa and MCF7) were fluorescently labeled with 25 μM CellTrackerTM Blue CMAC (InvitrogenTM) prior to preparing the cell mixture, whereas leukocytes were labeled with anti-CD45 FITC (InvitrogenTM). Whole blood samples were drawn from healthy volunteers into venous blood collection tubes (BD Vacutainer[®]) containing 0.4 ml of trisodium citrate (13.2 g/l), citric acid (4.8 g/l), and dextrose (14.7 g/l) and leukocytes were obtained by selectively lysing erythrocytes using RBC lysis buffer (eBioscience). Although cancer cells spiked in diluted whole blood can also be separated using microscale vortices, RBC-lysed blood was used in order to achieve practical throughput of cancer cell isolation. Blood and cancer cells were mixed to achieve a final ratio of 1:100 cancer cells to leukocytes. Cancer cell concentration used in this study was chosen to be relatively higher than the actual number counts reported for CTCs in clinical samples (e.g., 1–1000/1 ml of whole blood^{35,36}) for visualization and enumeration purposes. These experiments were performed with the total number concentration of 202 000 cells/ml and 1 ml of the cell solution was processed in each experiment.

C. Fluorescence and high-speed microscopic imaging

Microparticle/cell containing samples were injected into the device with a syringe pump (Harvard Apparatus, PHD 2000) to sustain an overall flow rate Q ranging between 10 $\mu\text{l}/\text{min}$ and 4.5 ml/min. The solution in a plastic syringe was continuously agitated during injection in order to maintain a uniform concentration throughout the experiment. The loaded syringe was connected to 1/32 \times 0.02 in. PEEK tubing (Upchurch Scientific) by a 1/2 in. luer stub (Instech Solomon) and tubing was secured in the punched inlet and outlet of the microfluidic device. Fluorescent images were recorded using a Nikon Eclipse Ti microscope equipped with a Photometrics CoolSNAP

HQ² charge-coupled device (CCD) camera and analyzed with Nikon NIS-ELEMENTS AR 3.0 software. Exposure time was varied from 5 to 30 s, according to the flow rate and observed fluorescence intensities. Three-dimensional vortex formation was visualized using a Nikon A1 Confocal microscope. High-speed microscopic images of trapping and releasing particle/cells were recorded downstream using Phantom v7.3 high-speed camera and Phantom Camera Control (Vision Research Inc.) and Phantom Camera Control software. All high speed images were taken using 1 μ s exposure time and image intervals were varied according to the flow rate.

D. Capturing efficiency and enrichment of larger cells using microscale-vortices

Various concentrations of fluorescently stained live HeLa cells as well as cancer cells spiked in dilute blood were loaded into the parallel microfluidic channel to evaluate the capturing efficiency as a function of cell concentrations. Prior to injection of the cell solutions, formation of microvortices at each reservoir was initiated and stabilized by flowing the flushing solution (i.e., growth media without cellular components) at $Q_{\text{flush}}=4.5$ ml/min for 30 s (vortex-priming step). The solution containing a known number of cells ($Q_{\text{cell}}=4$ ml/min) and a flushing solution ($Q_{\text{flush}}=0.5$ ml/min) were simultaneously injected through two separate inlets at the overall flow rate, $Q=Q_{\text{cell}}+Q_{\text{flush}}=4.5$ ml/min, to trap cancer cells in the reservoir (capturing step). Once a known amount of the cell solution was injected (0.5 or 1 ml), the cell solution was stopped ($Q_{\text{cell}}=0$) while the overall flow rate was maintained at 4.5 ml/min by increasing the flow rate of the flushing solution, Q_{flush} , in order to remove uncaptured cells from the device (flushing step). Finally, trapped cells were released from the reservoir by lowering Q_{flush} to 100 μ l/min until all captured cells escaped from reservoirs, followed by a 1 s final flush ($Q_{\text{flush}}=4$ ml/min) to ensure complete collection of cells released from the reservoir yet remaining in the tube (releasing step). Here, Q_{cell} and Q_{flush} were empirically optimized in order to ensure that the cell solution flows through all eight parallel channels during the capturing step, while backflow of the cell solution into the flushing inlet is prevented. Furthermore, during the vortex-priming, flush, and releasing steps, the flow of the cell solution through the sample inlet was physically stopped using a stopcock to prevent the additional introduction of unwanted, contaminating cells. Processed sample solutions at each step were collected separately in individual wells of a 48-well plate to determine the capturing efficiency, $\eta=(\text{Cancer})_{\text{captured}}/(\text{Cancer})_{\text{inlet}}$, by counting stained cells in fluorescence images taken over the entire well. Released cells collected in the 48-well plate were cultured over a week in a conventional CO₂ incubator to determine the viability of processed cancer cells. Furthermore, a mixed cell suspension of cancer cells spiked in dilute blood with or without lysed RBCs (cell solution) was flowed through the parallel microfluidic channel in order to isolate and enrich the larger cancer cells from the mixture following the same sample injection sequence. The enrichment ratio was determined as $\text{ER}=(\text{Cancer/Leukocytes})_{\text{outlet}}/(\text{Cancer/Leukocytes})_{\text{inlet}}$, using the number ratio between cancer and blood cells in collected samples and in the initial sample, obtained by counting stained cells in fluorescence images (N=10) taken at random locations.

IV. RESULTS AND DISCUSSION

A. Flow visualization and critical capturing diameter

Vortex structure and symmetry were found to be strongly dependent on flow speed. Figure 2(a) illustrates the two dimensional view of the evolution of the flow pattern within the reservoir, obtained using dilute fluorescent tracer particles ($a=1$ μ m). The detachment of the boundary layer was observed to be initiated at $R_c=21$ and the size of the vortex gradually increased with increasing flow rate. Moreover, it was found that the vortex core was progressively shifted toward the center of the reservoir and the microscale vortex finally occupied the entire reservoir at $R_c=215$ and remained stable for higher R_c . Interestingly, confocal microscopic images of 10 μ m fluorescent particle streaks revealed that the orbiting ring created by these trapped particles is located in between planes occupied by inertially focused particles in the straight region [Figs. 2(d) and 2(e)]. The ring occupies a region between the center and wall in the channel cross-section, but

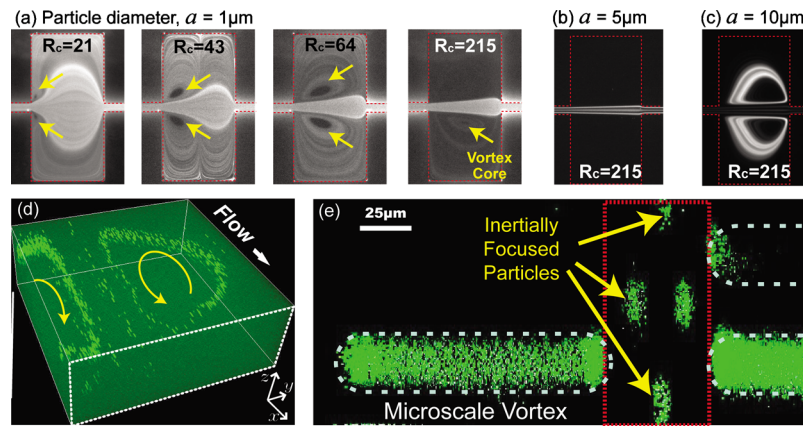


FIG. 2. Two- and three-dimensional flow pattern visualization and critical diameter determination. (a) Fluorescent microscopic images using dilute fluorescent particles ($a=1 \mu\text{m}$) illustrate the evolution of the flow pattern within the reservoir as flow rate increases. Trapped particle size cutoff was determined using dilute fluorescent particles ($a=5$ and $10 \mu\text{m}$). While (b) $5 \mu\text{m}$ particles freely pass through the reservoir, (c) $10 \mu\text{m}$ particles are trapped and recirculated within the reservoir. (d) Confocal fluorescent microscopic images describing the vortex formation in the cell trapping reservoir in three-dimensional and (e) its cross-sectional view.

further from the wall than the inertial focusing positions in the main channel. Notably, more than one vortex ring was observed to be formed in a single reservoir, suggesting multiple stable orbits that can be occupied by captured particles/cells. The fact that there are localized positions of the orbiting particles within the vortex may also be the result of inertial lift forces within the vortex. As the effective Reynolds number is less than that in the main channel, these particles would be expected to occupy positions further from the wall. Further investigations would be important to clarify this phenomenon.

In addition, we empirically found that particles/cells with diameter a greater than a critical diameter D_{crit} experience a shear-gradient lift force F_{LS} , which is strong enough to direct those particles into the reservoir. Experiments with fluorescent particles suggested that D_{crit} of the current device falls between 5 and $10 \mu\text{m}$ [Figs. 2(b) and 2(c)]. While trapping of $10 \mu\text{m}$ particles was initiated at $R_c=130$ and remained stable up to $R_c=240$, $5 \mu\text{m}$ fluorescence particles remained at focused streamlines in the main channel and were not trapped in the reservoir even for $R_c > 240$. Nonetheless, the critical diameter required for capturing live cells was found to be $17 \mu\text{m}$, greater than D_{crit} of rigid microspheres.³⁷ This could be attributed to the fact that deformable, intact cells tend to be focused closer to the channel center than rigid particles. Deformable cells experience an additional lift force toward the centerline in confined channels.^{38,39} Thus, a larger shear-gradient lift force (i.e., larger cell diameter) would be required to direct live cells into vortex required for successful trapping.

B. Massively parallel sized based particle/cell capturing using microscale vortices

The system was tested for the ability to enrich larger cells by flowing various concentrations of HeLa cells mixed with dilute human blood or suspended in culture medium. A simple two-inlet system allowed for easy and rapid solution exchange within the device, providing a means to flush untrapped smaller cells for enhancement of the final enrichment ratio and the purity of the collected samples [Figs. 3(a) and 3(b)]. Figure 3(c) shows the capturing efficiency as a function of the number of cancer cells introduced into the device for each run. The capturing efficiency decreased but remained higher than 25% as the number of cells introduced decreased (from 900 to 200 cells/run). Moreover, the capturing efficiency tends to agree with the value predicted from the cell size distribution of the introduced cell solution since 39% of HeLa cells were measured to have a cell diameter greater than $D_{\text{crit}}=17 \mu\text{m}$.⁴⁰ In addition, the capturing efficiency of the device was found to be lower than the average when the solution with a high cancer cell concentration (2000

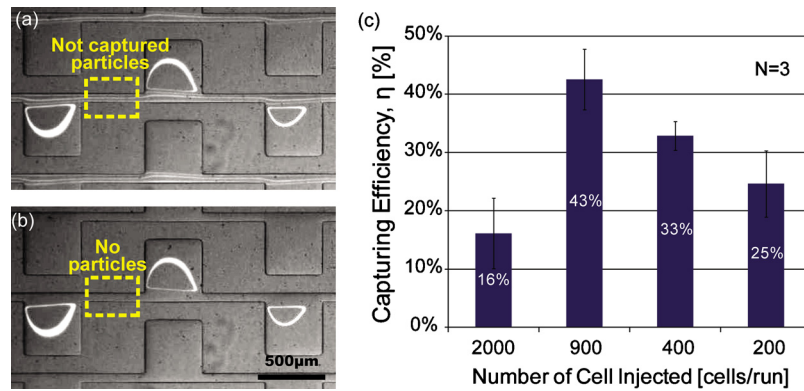


FIG. 3. Rapid solution exchange, yielding off-chip target cell collection with high purity. (a) 10 μm particles are trapped and recirculated within the reservoir when the sample solution is injected through the device at $R_c=242$. (b) Untrapped particles in the straight regions were flushed with deionized water by a rapid solution exchange mechanism once the bright rings in the reservoirs were observed. (c) Comparison of the capturing efficiency of the device as a function of cell concentration. The number of cells indicates the number of HeLa cells processed through the device.

cells/run) was introduced to the system. Presumably, such a high cell concentration exceeded the trapping capacity of the device (i.e., the maximum number of cells that each reservoir can trap and sustain). Based on our experiments, the maximum number of cells that each reservoir can effectively capture is estimated to range from 11 to 25 cells, depending on cell size. Furthermore, collected HeLa cells remained highly viable and proliferated for over a week, suggesting that the cell trapping mechanism using microscale vortices was not detrimental to normal function and growth.⁴⁰

As a proof of concept, using the significant difference in size between cancer and blood cells, we conducted label-free enrichment and collection of cancer cells [Figs. 4 and 5 (enhanced)]. Breast cancer cells (MCF7) were enriched by a factor of 7.1 with 23% capturing efficiency, while cervical cancer cells (HeLa) were enriched by 5.5 times with $\eta=10\%$. The lower ER and η of HeLa cells can be attributed to the smaller average cell size of HeLa cells ($a_{\text{ave}}=12.4 \mu\text{m}$) compared to that of MCF7 cells ($a_{\text{ave}}=20 \mu\text{m}$).^{41,42} Moreover, the reduction in η for the spiking experiments could result from (i) particle-particle interactions caused by the presence of high number of blood cells in the sample and/or (ii) a relatively higher number of cancer cells introduced the system (2000 cancer cells/run). In addition, given the preliminary nature of the current

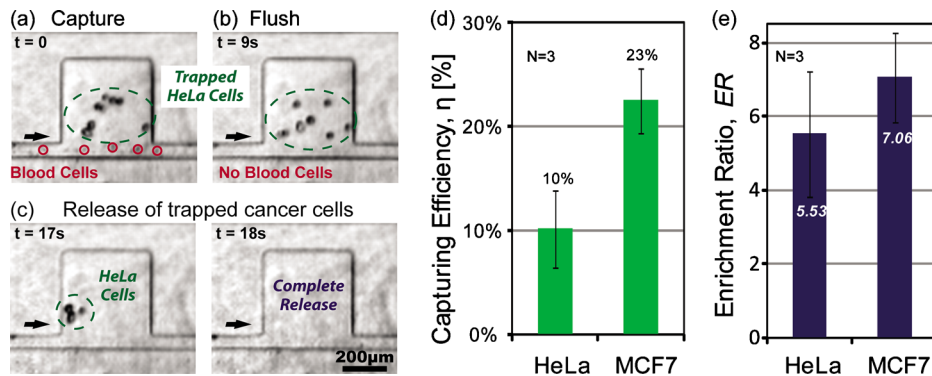


FIG. 4. Massively parallel large cell enrichment from blood using microscale vortices. (a) Dilute whole blood samples spiked with HeLa cells were injected into the device at $R_c=270$. (b) The device is flushed once the known volume of the cell solution has been flowed through the device. (c) The trapped HeLa cells were released from the reservoir by reducing the flow rate to achieve $R_c=5$ and collected off-chip for further analysis. (d) Capturing efficiency and (e) enrichment ratio of the system were found to be higher for MCF7 cells ($a_{\text{ave}}=20 \mu\text{m}$) than HeLa cells ($a_{\text{ave}}=12.4 \mu\text{m}$).^{41,42}

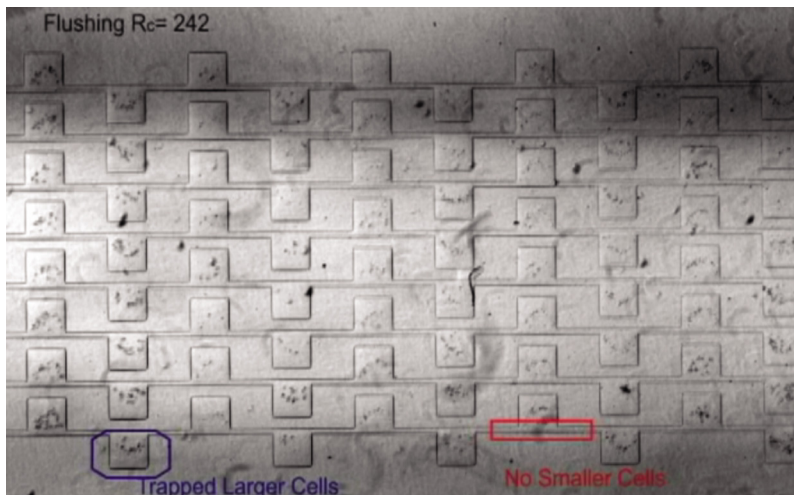


FIG. 5. Still image from video showing massively parallel large cell enrichment using microscale laminar vortex. MCF7 cells (breast carcinoma cell line) spiked in dilute whole blood (1% hematocrit) were enriched using a simple one layer microfluidic system. The real-time movie shows all 80 reservoirs effectively capture and release the larger cancer cell from dilute blood solution with a high throughput of 7.5×10^6 cells/s. The capturing and flushing steps in the movie were cropped in order to shorten overall play-time (enhanced online). [URL: <http://dx.doi.org/10.1063/1.3576780.1>]

studies, it is likely that the ER and η of the current technique can be further increased by changing the reservoir geometry from square to rectangle ($W_1 < W_2$) as (i) the size of vortices is expected to be larger and (ii) larger particle/cells will experience the shear-gradient lift force directed toward the vortex core for a longer duration.

The throughput of the current device is estimated to be 7.5×10^6 cells/s when the device is operated at $Re=242$ with dilute whole blood (1% hematocrit) and it can be further enhanced by simply parallelizing more channels or decreasing blood dilution factor. Indeed, the total throughput was increased by eightfold from 0.9 to 7.5×10^6 cells/s when eight single channels, each with ten reservoirs, were placed in parallel. This parallel device can concentrate larger, rare cells (e.g., CTCs) from 1 ml of peripheral blood and resuspend these cells into 860 nl of purified processed sample with the collected sample purity as high as 85% (i.e., more than *three orders of magnitude* increase in volumetric concentration factor). Here, the purity of the collected sample was determined from the number cell ratio between cancer and blood cells at the outlet. The ability to concentrate cells of interest in a small volume will enhance the overall throughput of current state-of-the-art image based target cell detection systems^{35,43} when the present device is integrated upfront of such systems. Additionally, integrating this system upfront of current cytopathology or immunocytochemistry⁴⁴ will expedite diagnostic and/or prognostic processes as the volume/area to be scanned/examined would be considerably reduced compared to current methods. It is still unclear whether the size of CTCs will correspond with those of cultured cancer cells, although reports have identified that cell size can be used as a biomarker for metastatic cells.^{8,43} Although the enrichment ratio and capturing efficiency of the current systems in these preliminary studies are considerably lower when compared to the state-of-art-techniques, the approach is label-free and simple with extreme throughput. The system's extreme throughput can compensate for efficiency in many cases by processing more samples to obtain the same amount or more number of cells. Similarly, simplicity of the system will allow massive parallelization and multiplex cascading of the target cell purifying processes for further enhancement of capturing efficiency and enrichment ratio. Furthermore, the presented label-free, sized-based target cell isolating technique would enable collection of viable, intact multicellular CTC-clusters, which could provide an important prognostic factor.³⁷

V. CONCLUSIONS

We have demonstrated a unique phenomenon, whereby laminar vortices act to selectively isolate particles above a critical cutoff size. Using this phenomenon, we have developed and evaluated an innovative microfluidic device for size-based cell isolation. The critical diameter of cells was found to be larger than that of rigid particles in agreement with effects from deformability induced lift forces arising in confined flow. Moreover, viable cancer cells spiked in dilute RBC-lysed blood were isolated and collected off-chip without compromising the capturing efficiency and the throughput. The presented technology improves on current technology by enriching cells based on size without clogging mechanical filters, employing only a simple single-layered microfluidic device and processing cell solutions at the ml/min scale. In contrast to filters, cells can also be easily released after capture in the vortices. The process is gentle, not adversely damaging cells, suggesting potential to enable cell enrichment by size from blood or tissue digests for future therapeutic uses and molecular analysis.

ACKNOWLEDGMENTS

The authors thank Karin Chen M.D., Jamie Powers M.D., Nicole K. Henderson-MacNennan and Professor Edward R.B. McCabe, M.D., Ph.D., for providing deidentified blood samples, Dennis J. Yoon and Professor Daniel T. Kamei, Ph.D., for instructing Coulter measurements, Jeffrey B. Huber for confocal fluorescent microscopy, and Youngjae Chun Ph.D. for help on experimental apparatus. This work was partially supported by Wallace H. Coulter Foundation Translational Research Award and National Science Foundation under Grant No. 0930501.

- ¹S. Harding, N. Ali, M. Brito-Martins, and J. Gorelik, *Pharmacol. Ther.* **113**, 341 (2007).
- ²M. Laflamme, K. Chen, A. Naumova, V. Muskheli, J. Fugate, S. Dupras, H. Reinecke, C. Xu, M. Hassanipour, and S. Police, *Nat. Biotechnol.* **25**, 1015 (2007).
- ³D. Anderson, T. Self, I. Mellor, G. Goh, S. Hill, and C. Denning, *Mol. Ther.* **15**, 2027 (2007).
- ⁴D. Cha, K. Khosrotehrani, D. Bianchi, and K. Johnson, *Prenat. Diagn.* **25**, 586 (2005).
- ⁵M. Taylor, J. Rössler, B. Georger, A. Laplanche, O. Hartmann, G. Vassal, and F. Farace, *Clin. Cancer Res.* **15**, 4561 (2009).
- ⁶M. Cristofanilli, G. Budd, M. Ellis, A. Stopeck, J. Matera, M. Miller, J. Reuben, G. Doyle, W. Allard, and L. Terstappen, *N. Engl. J. Med.* **351**, 781 (2004).
- ⁷D. R. Gossett, W. M. Weaver, A. J. Mach, S. C. Hur, H. T. Tse, W. Lee, H. Amini, and D. Di Carlo, *Anal. Bioanal. Chem.* **397**, 3249 (2010).
- ⁸S. Zheng, H. Lin, J. Liu, M. Balic, R. Datar, R. Cote, and Y. Tai, *J. Chromatogr., A* **1162**, 154 (2007).
- ⁹M. Yamada, M. Nakashima, and M. Seki, *Anal. Chem.* **76**, 5465 (2004).
- ¹⁰J. Green, M. Radisic, and S. Murthy, *Anal. Chem.* **81**, 9178 (2009).
- ¹¹J. Davis, D. Inglis, K. Morton, D. Lawrence, L. Huang, S. Chou, J. Sturm, and R. Austin, *Proc. Natl. Acad. Sci. U.S.A.* **103**, 14779 (2006).
- ¹²R. Huang, T. Barber, M. Schmidt, R. Tompkins, M. Toner, D. Bianchi, R. Kapur, and W. Flejter, *Prenat. Diagn.* **28**, 892 (2008).
- ¹³S. Choi, S. Song, C. Choi, and J. Park, *Anal. Chem.* **81**, 1964 (2009).
- ¹⁴D. Di Carlo, D. Irimia, R. G. Tompkins, and M. Toner, *Proc. Natl. Acad. Sci. U.S.A.* **104**, 18892 (2007).
- ¹⁵D. Di Carlo, J. F. Edd, D. Irimia, R. G. Tompkins, and M. Toner, *Anal. Chem.* **80**, 2204 (2008).
- ¹⁶A. J. Mach and D. Di Carlo, *Bioengineering and Biotechnology* **107**, 302 (2010).
- ¹⁷H. Moffatt, *J. Fluid Mech.* **18**, 1 (1964).
- ¹⁸W. Cherdron, F. Durst, and J. Whitelaw, *J. Fluid Mech.* **84**, 13 (1978).
- ¹⁹T. Karino and H. Goldsmith, *Microvasc. Res.* **17**, 217 (1979).
- ²⁰T. Karino and H. Goldsmith, *Philos. Trans. R. Soc. London, Ser. B* **279**, 413 (1977).
- ²¹E. O. Macagno and T. Hung, *J. Fluid Mech.* **28**, 43 (1967).
- ²²F. Laine-Pearson and P. Hydon, *Stud. Appl. Math.* **122**, 139 (2009).
- ²³D. Lim, J. Shelby, J. Kuo, and D. Chiu, *Appl. Phys. Lett.* **83**, 1145 (2003).
- ²⁴Marcos and R. Stocker, *Limnol. Oceanogr. Methods* **4**, 392 (2006).
- ²⁵E. Sollier, M. Cubizolles, Y. Fouillet, and J. Achard, *Biomed. Microdevices* **12**, 485 (2010).
- ²⁶J. Park and H. Jung, *Anal. Chem.* **81**, 8280 (2009).
- ²⁷D. Chiu, *Anal. Bioanal. Chem.* **387**, 17 (2006).
- ²⁸C. Lin, Y. Lai, H. Liu, C. Chen, and A. Wo, *Anal. Chem.* **80**, 8937 (2008).
- ²⁹M. Khabiry, B. Chung, M. Hancock, H. Soundararajan, Y. Du, D. Cropek, W. Lee, and A. Khademhosseini, *Small* **5**, 1186 (2009).
- ³⁰J. Matas, J. Morris, and E. Guazzelli, *J. Fluid Mech.* **515**, 171 (1999).
- ³¹D. Di Carlo, J. Edd, K. Humphry, H. Stone, and M. Toner, *Phys. Rev. Lett.* **102**, 094503 (2009).
- ³²S. C. Hur, H. T. K. Tse, and D. Di Carlo, *Lab Chip* **10**, 274 (2010).
- ³³E. Asmolov, *J. Fluid Mech.* **381**, 63 (1999).

- ³⁴D. Duffy, J. McDonald, O. Schueller, and G. Whitesides, *Anal. Chem.* **70**, 4974 (1998).
- ³⁵S. Nagrath, L. Sequist, S. Maheswaran, D. Bell, D. Irimia, L. Ulkus, M. Smith, E. Kwak, S. Digumarthy, and A. Muzikansky, *Nature (London)* **450**, 1235 (2007).
- ³⁶R. Krivacic, A. Ladanyi, D. Curry, H. Hsieh, P. Kuhn, D. Bergsrud, J. Kepros, T. Barbera, M. Ho, and L. Chen, *Proc. Natl. Acad. Sci. U.S.A.* **101**, 10501 (2004).
- ³⁷B. Molnar, A. Ladanyi, L. Tanko, L. Sréter, and Z. Tulassay, *Clin. Cancer Res.* **7**, 4080 (2001).
- ³⁸C. K. W. Tam and W. Hyman, *J. Fluid Mech.* **59**, 177 (1973).
- ³⁹S. C. Hur, N. K. Henderson-MacLennan, E. R. B. McCabe, and D. Di Carlo, *Lab Chip* **11**, 912 (2011).
- ⁴⁰See supplementary material at <http://dx.doi.org/10.1063/1.3576780> for size distribution of HeLa cells captured using the device and viability of captured cells.
- ⁴¹G. Gobert and H. Schatten, *J. Electron Microsc.* **49**, 539 (2000).
- ⁴²K. Rafferty, *Virchows Arch. B Cell Pathol.* **50**, 167 (1986).
- ⁴³D. Marrinucci, K. Bethel, M. Luttgen, R. Bruce, J. Nieva, and P. Kuhn, *Arch. Pathol. Lab. Med.* **133**, 1468 (2009).
- ⁴⁴P. Fetsch, K. Cowan, D. Weng, A. Freifield, A. Filie, and A. Abati, *Diagn. Cytopathol.* **22**, 323 (2000).